

Current disruption and its spreading in collisionless magnetic reconnection

Neeraj Jain,^{1,2} Jörg Büchner,^{1,2} Seth Dorfman,³ Hantao Ji,^{1,4} and A. Surjalal Sharma⁵

¹Max-Planck/Princeton Center for Plasma Physics

²Max Planck Institute for Solar System Research, 37191 Katlenburg-Lindau, Germany

³University of California Los Angeles, Los Angeles, California 90095, USA

⁴Department of Astrophysical Sciences and Princeton Plasma Physics Laboratory, Princeton University, Princeton, New Jersey 08540, USA

⁵Department of Astronomy, University of Maryland, College Park, Maryland 20742, USA

(Received 29 August 2013; accepted 15 October 2013; published online 4 November 2013)

Recent magnetic reconnection experiments (MRX) [Dorfman *et al.*, *Geophys. Res. Lett.* **40**, 233 (2013)] have disclosed current disruption in the absence of an externally imposed guide field. During current disruption in MRX, both the current density and the total observed out-of-reconnection-plane current drop simultaneously with a rise in out-of-reconnection-plane electric field. Here, we show that current disruption is an intrinsic property of the dynamic formation of an X-point configuration of magnetic field in magnetic reconnection, independent of the model used for plasma description and of the dimensionality (2D or 3D) of reconnection. An analytic expression for the current drop is derived from Ampere's Law. Its predictions are verified by 2D and 3D electron-magnetohydrodynamic (EMHD) simulations. Three dimensional EMHD simulations show that the current disruption due to localized magnetic reconnection spreads along the direction of the electron drift velocity with a speed which depends on the wave number of the perturbation. The implications of these results for MRX are discussed. © 2013 AIP Publishing LLC. [<http://dx.doi.org/10.1063/1.4827828>]

I. INTRODUCTION

Reconnection is the dominant mechanism of often explosive releases of magnetic energy in astrophysical and laboratory plasmas. Magnetic reconnection involves space and time scales ranging from the small electron scales to large magnetohydrodynamic (MHD) fluid scales. In the last six decades, studies of magnetic reconnection employing first theoretical methods^{1–5} and later computer simulations^{6–9} have made several advances toward a better understanding of the physics of magnetic reconnection and a fast release of magnetic energy. In collisionless plasmas, the scale length of the dissipation region, in which the frozen-in condition of magnetic field breaks down allowing reconnection, becomes comparable to the intrinsic microscopic lengths, viz., ion inertial length $d_i = c/\omega_{pi}$ and even the electron inertial length $d_e = c/\omega_{pe}$. This invalidates a MHD description and requires a multi-species or even kinetic description of the plasma. The motion of the electrons and ions decouples in the dissipation region forming an electron scale current sheet (thickness $\sim d_e$) embedded inside an ion scale current sheet (thickness $\sim d_i$). In reconnection models without guide field, this generates a quadrupolar structure of the out-of-plane magnetic field.^{10,11} The formation of a multi-scale structure and quadrupole out-of-plane magnetic field has been confirmed by satellite observations in space and by laboratory experiments.^{12–15}

In impulsive reconnection events, the current density has been observed to drop suddenly following a long period of its build-up. For example, the cross tail current density in the Earth's magnetotail first slowly increases before the onset of sub-storms and then drops fast. This drop in the current was termed current disruption.^{16–18} Current disruption in laboratory experiments revealed that it is accompanied by

an enhanced reconnection.^{19–22} For example, merging spheromak experiments in counter helicity mode show that an ejection of the current density is associated with a sudden increase of the reconnection rate.²²

In this paper, we focus on the physics of current disruption and its relation to magnetic reconnection. We also investigate the spreading of localized reconnection and the associated current disruption in the direction of current. It should be noted that the present paper does not address the mechanism(s) responsible for impulsive reconnection which should include both the slow build up and fast disruption phases.

Our studies are motivated by recent observations of localized 3D current disruption events in laboratory magnetic reconnection experiments (MRX).²¹ These experiments have shown that after a slow build up phase, the reconnection electric field at the X-point rises simultaneously with both a drop in the current density at the X-point and a decrease in total current integrated over the probe coverage area. The current disruption events observed in MRX are attributed to the ejection of a flux rope (O-point in the reconnection plane) from the plane of reconnection leaving behind an X-point structure. This broadens the anti-parallel magnetic field profile across the thickness of the current sheet in the reconnection plane. The broadening of the magnetic field profile spreads in the direction of the electron drift.

Here, we distinguish between the usage of the term “current disruption” to describe a drop either in current density or in the total integrated current. The term “current disruption” has mainly been used in context of current disruption in the Earth's magnetosphere, defined as a sudden drop in current density rather than the total integrated current.¹⁷ While this is consistent with the definition used in MRX experiments, the total current integrated over the probe

coverage area is also observed to drop. However, it is possible to construct a situation where a drop in the local current density does not occur simultaneously with a drop in total integrated current. For example, the current density may evolve to a turbulent state in which regions of drop and enhancement of the current density are randomly distributed in space and time. In this case, a single dominant X-point, at which current density should be measured, cannot be clearly identified. Another possibility is that the current density drops everywhere but spreads over a wider region such that the total current remains the same or even increases. However, due to the limited observations in the Earth's magnetosphere, it may not be possible to calculate the total current. Therefore, we distinguish between the two cases by calling the drop of current density "localized current disruption" and drop of total current "global current disruption." In this paper, we shall use the term "current disruption" to describe the global current disruption in which the total out-of-reconnection-plane current, obtained by integrating current density over a region surrounding an X-point, drops and the out-of-reconnection-plane electric field at X-point rises.

In this paper, we first show that current disruption is an inherent property of the dynamic formation of an X-point magnetic field configuration during reconnection. This result is independent of the model used for the plasma description and the dimensionality (2D or 3D) of reconnection. We derive an analytic expression for the current drop directly from first principles, starting with a typical X-point magnetic field configuration without referring to the dimensionality. This means that the current disruption can occur both in 2D and 3D. The MRX experiments²¹ show examples of 3D current disruptions. In the MRX experiments,²¹ current disruption occurs when a flux rope is ejected in 3D fashion, leaving behind an X-point magnetic field configuration. Two and three dimensional simulations of reconnection are performed using an electron-MHD (EMHD) model to illustrate how current disruption occurs in 2D as well as in 3D. The expression of the amount of the current drop is verified both by 2D and 3D EMHD simulations.

On the other hand, the spreading of the current disruption in the direction perpendicular to the initial reconnection plane is a 3D phenomenon. In MRX,²¹ e.g., the half thickness of the current sheet before the current disruption was $\approx 1 \text{ cm} \approx 6-7d_e$. The duration of the current disruption was $\approx 4 \mu\text{s} \approx \omega_{ci}^{-1}$. The current disruption spread over the toroidally resolved region ($\approx 10 \text{ cm}$) in $\approx 2 \mu\text{s} \approx 0.5\omega_{ci}^{-1}$ (see Fig. 4 of Dorfman *et al.*²¹), giving speed of spreading $\approx 5 \text{ cm}/\mu\text{s}$. This indicates that the physics of current disruption in this experiment is dominated by the electrons. Therefore, it is appropriate to investigate the spreading of the current disruption by performing 3D EMHD simulations. Note that although the EMHD simulations presented in this paper do not directly correspond to the experimental setup of MRX, they indicate that the electron dynamics governs the physics of MRX reconnection. While EMHD does not describe kinetic effects, it nevertheless captures many essential details of the electron-dominated reconnection processes. EMHD simulations show, e.g., that the current disruption due to localized reconnection spreads in the electron drift direction with a speed which depends on

the wavenumber of the perturbation that caused the reconnection. The wave number dependence allows the speed of spreading to be much smaller than the speed of the current carriers. Note that this new result is consistent with the MRX experiments²¹ in which it was found that the speed of spreading is much smaller than the speed of the current carriers. Earlier theoretical and simulation results found that the speed of spreading is very close to the speed of the current carriers^{23,24} or to the wave velocity of the generating sausage or drift waves.^{25,26} These studies, however, did not consider the wave number dependence of the speed of spreading. We show that the speed of spreading can vary from a fraction of the current carrier (electrons in present studies) speed to the current carrier speed depending on wave numbers.

The paper is organized as follows. Section II describes the EMHD model and the simulation setup. In Sec. III, we obtain an analytic expression for the current drop due to reconnection. It is verified by means of 2D EMHD simulations. Section IV presents 3D EMHD simulations of the spreading of the current disruption in the direction of the electron drift. In Sec. IV, the expression of current drop is verified again also by 3D EMHD simulations. A numerical solution of linear EMHD equations to obtain the wave number dependence of the speed of the spreading is presented in Sec. IV. Finally, conclusions and discussions of the results in the context of the MRX reconnection experiment are given in Sec. V.

II. EMHD MODEL AND SIMULATION SETUP

The EMHD model describes the dynamics of the electron fluid in a stationary background of ions. It is valid for spatial scales smaller than d_i and time scales smaller than ω_{ci}^{-1} . The EMHD equations are obtained by eliminating the electric field from the electron momentum equation using Faraday's law. They can be written as²⁷

$$\frac{\partial}{\partial t}(\mathbf{B} - d_e^2 \nabla^2 \mathbf{B}) = \nabla \times [\mathbf{v}_e \times (\mathbf{B} - d_e^2 \nabla^2 \mathbf{B})], \quad (1)$$

$$\mathbf{v}_e = -\frac{1}{\mu_0 n_0 e} \nabla \times \mathbf{B}. \quad (2)$$

In addition to ignoring the ion dynamics, Eqs. (1) and (2) assume uniform electron number density n_0 and incompressibility of the electron fluid. The displacement current is ignored under the assumption $\omega \ll \omega_{pe}^2/\omega_{ce}$.

In EMHD, the frozen-in condition of magnetic field breaks down due to the electron inertia (which is contained in the two terms with Laplacian operator in Eq. (1)) leading to reconnection. In the absence of electron inertia, Eq. (1) represents the condition that the magnetic field is frozen in the electron fluid. Electron inertia is the dominant non-ideal term in Ohm's law for fast time-dependent phenomena in very thin current sheets (thickness $\sim d_e$).²⁸ This is in contrast with the steady state of reconnection in which divergence of the electron pressure tensor is the dominant term in the generalized Ohm's law of collisionless two-fluid plasmas.²⁸⁻³⁰

The equilibrium magnetic field is taken to be $\mathbf{B}_0 = B_\infty \tanh(x/L) \hat{z}$ (x will be referred to as radial direction in this paper) corresponding to a current density $\mathbf{J}_0 = -(B_\infty/$

$\mu_0 L \text{sech}^2(x/L) \hat{y}$, where $L = d_e$ is the half thickness of the current sheet. For stationary ions, this means $\mathbf{J}_0 = -n_0 e \mathbf{v}_e$.

Similar to the Geospace Environment Modeling (GEM) reconnection challenge,⁶ simulations are initialized by a high amplitude perturbation with a purpose of initially forming an X-point configuration of the magnetic field. These initial conditions avoid waiting for a spontaneous onset of reconnection. The perturbation has the form

$$\tilde{B}_x(x, y, z) = B_{x1} \exp(-x^2/L^2) g(y) \sin(\pi z/l_z), \quad (3)$$

with $B_{x1} = 0.1B_\infty$. Such a perturbation forms a single X-point in the center of the coordinate frame, where it triggers reconnection. For 2D simulations, $g(y) = 1$ while for 3D perturbations, two choices of $g(y)$ are used corresponding to (1) a y -localized perturbation and (2) a sinusoidal perturbation with a single wavelength along y . The simulation box extends from $x = -l_x$ to l_x and $z = -l_z$ to l_z in 2D case. In the 3D case, it extends along y as well from $y = -l_y$ to l_y . The boundary conditions are periodic along y and z while the perturbations vanish at x boundaries far away from the central region of interest.

For 2D simulations, the box size ($2l_x \times 2l_z$) is $60d_e \times 15d_e$ with 400×100 grid points. For 3D simulations, the box sizes ($2l_x \times 2l_y \times 2l_z$) are $10d_e \times 10d_e \times 80d_e$ with $40 \times 40 \times 320$ grid points for y -localized perturbation and $20d_e \times 20d_e \times 20d_e$ with $80 \times 80 \times 80$ grid points for the sinusoidal perturbation in y . The time step for all the simulations is $\omega_{ce} \Delta t = 0.01$.

Results (except the derivation of the expression for the current-drop in Sec. III A) will be presented using the following normalization: The magnetic field is normalized by its asymptotic value B_∞ , length by the electron skin depth d_e , time by the inverse electron cyclotron frequency $\omega_{ce}^{-1} = (eB_\infty/m_e)^{-1}$, and velocity by the electron Alfvén velocity $v_{Ae} = d_e \omega_{ce}$. Under this normalization, $\mathbf{J}_0 = -\mathbf{v}_e$.

III. CURRENT DISRUPTION

A. Derivation

Let us consider a typical initial current layer configuration with an imposed magnetic reconnection perturbation. A current layer carrying current along the y direction and confined along x produces an anti-parallel magnetic field B_z which changes its direction at $x = x_0$ (at which point the layer is centered). We wish to calculate the evolution of the total current along y through an area around the X-point in the x - z plane after the initially anti-parallel magnetic field lines start to reconnect. The projection of magnetic field lines in the x - z plane, shown in Fig. 1, depicts a typical magnetic field configuration near an X-point valid in 2D and 3D reconnection. Here, we use the physical un-normalized quantities to derive an expression for the current drop.

The total current along y through an area in x - z plane ($x_1 < x < x_2, z_1 < z < z_2$) can be written as $I_{y,\text{total}}(t) = (1/\mu_0) \int_{x_1}^{x_2} \int_{z_1}^{z_2} \hat{y} \cdot \nabla \times \mathbf{B} dx dz = I_{y1}(t) + I_{y2}(t)$, where

$$I_{y1}(t) = -\frac{1}{\mu_0} \int_{z_1}^{z_2} dz [B_z(x_2, z, t) - B_z(x_1, z, t)] \quad \text{and}$$

$$I_{y2}(t) = \frac{1}{\mu_0} \int_{x_1}^{x_2} dx [B_x(x, z_2, t) - B_x(x, z_1, t)]$$

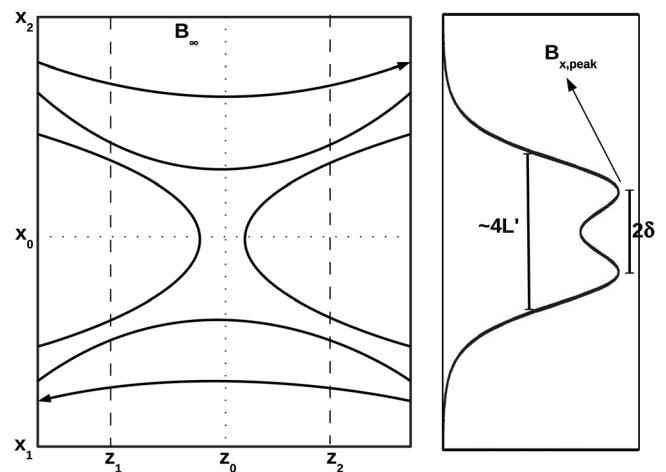


FIG. 1. (Left) Geometry of reconnecting magnetic field lines in the x - z plane for the calculation of the total current $I_{y,\text{total}}$ through the area $x_1 < x < x_2$ and $z_1 < z < z_2$. (Right) Shape of a typical eigen-function for B_x in evolving reconnection.

are the currents due to the x -variation of the reconnecting magnetic field B_z and the z -variation of the reconnected magnetic field B_x , respectively. The initial magnetic field, assumed to have a profile $B_z(x, z, t = 0) = B_\infty \tanh[(x - x_0)/L]$, changes around the center ($x = x_0$) of the current sheet as reconnection proceeds. At the same time, it remains more or less constant far away ($|x - x_0| \gg L$) from the center of the sheet. Taking $x_0 - x_1, x_2 - x_0 \gg L$, $B_z(x_1, z, t) = -B_\infty$ and $B_z(x_2, z, t) = B_\infty$. This gives

$$I_{y1} = -\frac{2}{\mu_0} B_\infty (z_2 - z_1), \quad (4)$$

which does not depend on time. Since $I_{y2}(t = 0) = 0$ (no reconnected field at $t = 0$), $I_{y1} = I_{y,\text{total}}(t = 0)$ is the initial total current.

In the course of reconnection, the magnetic field is changing away from $B_z(x, z, t = 0) = B_\infty \tanh[(x - x_0)/L]$. Reconnection at the site (x_0, z_0) forms an X-point configuration of the magnetic field, generating the reconnected field $B_x(x, z_2, t) > 0$ for $z_2 > z_0$ and $B_x(x, z_1, t) < 0$ for $z_1 < z_0$. Therefore, $I_{y2}(t) > 0$ and magnitude of the total current $I_{y,\text{total}} = I_{y1} + I_{y2}$ drops as a result of the evolution of X-point configuration of magnetic field.

Around (x_0, z_0) , the reconnected field B_x is an anti-symmetric function of z . Taking the limits z_1 and z_2 to be equidistant from z_0 on the two sides of the reconnection site ($z_0 - z_1 = z_2 - z_0$), $B_x(x, z_2, t) = -B_x(x, z_1, t)$, and therefore,

$$I_{y2}(t) = \frac{2}{\mu_0} \int_{x_1}^{x_2} B_x(x, z_2, t) dx$$

To quantitatively estimate the current drop, the shape of $B_x(x, z_2, t)$ can be approximated as a typical shape of the eigen function of the reconnecting field (Fig. 1, right panel: two peaks separated by a small distance and a dip at $x = x_0$) using the function

$$B_x(x, z_2, t) = B_{x0}(z_2, t) \left[\operatorname{sech}^2 \left(\frac{x - x_0 - \delta}{L'} \right) + \operatorname{sech}^2 \left(\frac{x - x_0 + \delta}{L'} \right) \right], \quad (5)$$

where

$$B_{x0}(z_2, t) = \frac{B_{x,peak}(z_2, t)}{1 + \operatorname{sech}^2(2\delta/L')} > 0.$$

Here, $B_{x,peak}$ is the peak value, 2δ is the distance between the two peaks, and $2L' \sim 2\delta$ is approximately the half width of the eigen function. Using Eq. (5)

$$I_{y2}(t) = \frac{8L'}{\mu_0} \frac{B_{x,peak}(z_2, t)}{1 + \operatorname{sech}^2(2\delta/L')}. \quad (6)$$

Hence, using $\operatorname{sech}^2(2\delta/L') \ll 1$ for $\delta \sim L'$ the fractional change in the total current $(\Delta I_{y,total})_f = \Delta I_{y,total}(t)/I_{y,total}(t=0)$ can be obtained as

$$\begin{aligned} (\Delta I_{y,total})_f &= \frac{I_{y,total}(t=0) - I_{y,total}(t)}{I_{y,total}(t=0)} \\ &= \frac{B_{x,peak}(z_2, t)}{B_\infty} \times \frac{4L'}{(z_2 - z_1)}. \end{aligned} \quad (7)$$

Note that $(\Delta I_{y,total})_f$ is directly proportional to $B_{x,peak}(z_2, t)$. Hence, $I_{y,total}(t)$ keeps dropping with the rise in $B_{x,peak}(z_2, t)$. It must saturate, i.e., stop changing in time with the saturation of $B_{x,peak}(z_2, t)$. Amplitude and spatio-temporal scales in the saturated state may depend on physical plasma model, external drive, physical parameters, and dimensionality of the system. For example, in the EMHD model, the initial thickness L of the current sheet affects the saturated state. Thinner current sheets have more free energy and reconnection grows faster compared to the thicker current sheets. Therefore, in case of spontaneous reconnection, thinner current sheets can quickly drive the system to a high level of saturation amplitude, and hence cause a larger and faster drop in the total current.

In order that Eq. (7) gives an amount of drop in the total current ($[\Delta I_{y,total}]_f > 0$), $B_x(x, z_2, t) > 0$. Therefore, while applying Eq. (7), one should choose a value of z_2 such that $B_x(x, z_2, t) > 0$. In case of a single X-point $B_x(x, z_2, t) > 0$ for all values of z_2 , therefore, any value of z_2 can be chosen. However, in case of multiple X-points, $B_x(x, z_2, t)$ changes sign at certain values of z_2 . In this case, a value of z_2 should be chosen so that $B_x(x, z_2, t) > 0$ making $[\Delta I_{y,total}]_f > 0$. Note that, although Eq. (7) was derived assuming $B_x(x, z_2, t) > 0$, it is valid even in a case of $B_x(x, z_2, t) \leq 0$ giving an amount of rise instead of drop in the total current. It means that in case of multiple X-points, the rise or drop in the total current depends on the region of integration. The total current drops (rises) with time as long as the region of integration contains more X-points (O-points) than O-points (X-points). Our objective in this paper is to demonstrate that dynamic formation of an X-point is always associated with a drop in the total current. Therefore, while verifying Eq. (7)

with EMHD simulations in Secs. III B and IV A, we choose our region of integration to contain a single X-point.

According to Faraday's law, the rise in $B_{x,peak}(z_2, t)$ due to the generation of the reconnected magnetic field must lead to a rise in the inductive electric field E_y at the X-point. This electric field is expected to peak around the time when $dB_{x,peak}/dt$ is maximum. The current $I_{y,total}$ also drops fastest at the maximum of $dB_{x,peak}/dt$ (see Eq. (7)). Hence the instants of time, at which peak in E_y (at the X-point) and fastest drop in current occur, are related. The peak of E_y falls near the ankle (where the current begins to drop slowly after a period of fastest drop) of the current drop curve $I_{y,total}(t)$ vs. t . The total current finally saturates with the saturation of $B_{x,peak}$.

Equation (7) assumes $B_{xi}(z_2) = B_{x,peak}(z_2, t=0) = 0$. If $B_{xi}(z_2)$ is finite, $I_{y2}(t=0)$ will be finite and contribute to total initial current. In this case, the expression for fractional change in current becomes

$$(\Delta I_{y,total})'_f = (\Delta I_{y,total})_f \left[\frac{1 - \frac{L'_0}{L'} \frac{B_{xi}(z_2)}{B_{x,peak}(z_2, t)}}{1 - \frac{4L'_0}{z_2 - z_1} \frac{B_{xi}(z_2)}{B_\infty}} \right], \quad (8)$$

where $2L'_0$ is the initial half width of the eigen function and $(\Delta I_{y,total})_f$ can be calculated using Eq. (7). Although the fractional change in current at a given time t , given by Eq. (8), in general, depends on the initially finite B_x through B_{xi} and L'_0 , it becomes independent of initial B_x if $B_{xi}(z_2) \ll B_{x,peak}(z_2, t), B_\infty$ and $L'_0 \ll L', (z_2 - z_1)/4$. Physically, it means that by time t the amplitude and radial scale of $B_x(x, z_2, t)$ must grow to values much larger than their initial values. In addition, the initial values of the amplitude and the radial scale of $B_x(x, z_2, t)$ must be much smaller than the asymptotic value of the reconnecting magnetic field and $z_2 - z_1$, respectively. For sufficiently small B_{xi} and L'_0 , the expression for $(\Delta I_{y,total})'_f$ can be simplified using a binomial expansion and neglecting terms which are second order in small quantities

$$(\Delta I_{y,total})'_f = (\Delta I_{y,total})_f \left[1 - \frac{L'_0 B_{xi}(z_2)}{L' B_{x,peak}(z_2, t)} \{1 - (\Delta I_{y,total})_f\} \right]. \quad (9)$$

It can be seen that for $(\Delta I_{y,total})_f < 1$, increasing the values of $B_{xi}(z_2)$ or L'_0 reduces $(\Delta I_{y,total})'_f$.

B. Verification by simulations

Let us first verify Eq. (7) for the current drop by 2D EMHD simulations. (The same expression will be verified by 3D simulations later in Sec. IV A.) Fig. 2 shows the magnitude of the total out-of-plane current $I_{y,total}(t) = \int_{-l_x}^{l_x} \int_{-l_z/2}^{l_z/2} J_y(x, z, t) dx dz$, obtained directly from 2D EMHD simulations. Also shown in Fig. 2 is $|I_{y,total}| = |I_{y1} + I_{y2}|$, where I_{y1} and I_{y2} are calculated using normalized versions of Eqs. (4) and (6). For estimation of the values of L' , $B_{x,peak}$ and δ , the simulation profiles of $B_x(x, l_z/2, t)$, shown in Fig. 2, are

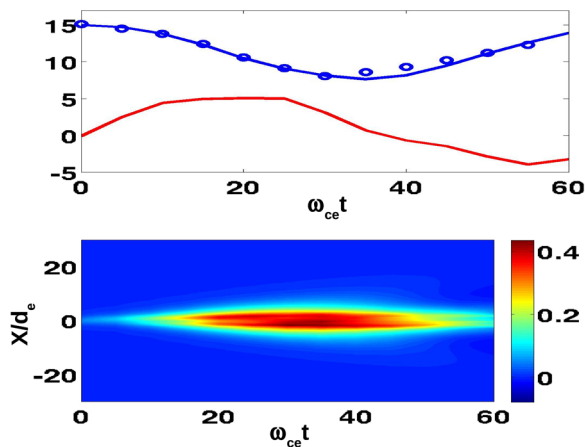


FIG. 2. (Top panel) Electric field ($-E_y \times 100$, red line) at the X-point, magnitude of the total current along y calculated directly from the simulations (blue line), and from $|I_{y,\text{total}}| = |I_{y1} + I_{y2}|$ using normalized versions of Eqs. (4) and (6) (blue circle). (Bottom panel) Simulation profile of $B_x(x, l_z/2, t)$ used to estimate L' , δ , and $B_{x,\text{peak}}$ in Eq. (6).

used. The current drops almost by 50% by $\omega_{ce}t = 30$. Simultaneously, the magnitude of E_y rises to its peak value near the ankle of the current drop. After that, the magnitude of E_y drops again. There is a close agreement between the current calculated directly by the simulation and the current calculated using the analytic expressions.

Note that expression (7) for the current drop was derived using Ampere's law simply considering a typical X-point geometry of a reconnection magnetic field. It does not require considerations either of dimensionality (2D or 3D) or of a specific model of plasma description. Note that, although the fractional amount of current drop in expression (7) depends on the chosen shape for the eigen function $B_x(x, z_2, t)$, the current disruption occurs independent of the shape of the eigen-function. The main reason for the current disruption is that the reconnected magnetic field, independent of its radial shape, always corresponds to a current I_{y2} in the direction opposite to the initial current I_{y1} . Therefore, as long as $I_{y1}I_{y2} < 0$, the magnitude of the total current always drops in reconnection for any radial shape of the reconnected magnetic field $B_x(x, z_2, t)$. The opposite signs of I_{y1} and I_{y2} are not specific to the chosen magnetic field geometry for which $I_{y1} < 0$ and $I_{y2} > 0$. If we reverse the direction of B_z , the signs of both I_{y1} and I_{y2} will be reversed as well. Therefore, we conclude that current disruption is an intrinsic property of the dynamic formation of an X-point magnetic field configuration in reconnection. Duration and amount of current disruption will, off course, depend on the physical mechanism allowing magnetic reconnection. The physical mechanism may depend on the physical parameters, applicable plasma model and the dimensionality. A detailed study of the dependence of current disruption on physical parameters, plasma model and dimensionality will be presented in future publications. Here we demonstrate current disruption and its spreading in the framework of an EMHD model.

IV. SPREADING OF CURRENT DISRUPTION

In three dimensions, current disruption is expected to spread perpendicular to the initial reconnection plane.

Although the occurrence of current disruption itself does not require any specific dimensionality (2D or 3D) or plasma model, its spreading does require three dimensional geometry and may well depend on plasma model. We study the spreading of the current disruption by performing 3D EMHD simulations.

A. y -Localized perturbation

First, we initialized the simulations with a perturbation localized in y , i.e., we choose a shape function $g(y) = 0.5 [\tanh(y/d_e + 35) - \tanh(y/d_e + 5)]$ which rises from $g = 0$ at $y = 0$ to $g = 1$ at $y \approx -7.5d_e$. Such perturbation remains uniform at $g = 1$ for $-7.5 > y/d_e > -32.5$ and then drops to $g = 0$ at $y/d_e = -40$. Reconnection triggered by this perturbation initially forms an X-line $x = z = 0$ along y in the whole region of the localization ($-40 < y/d_e < 0$) of the initial perturbation. This broadens B_z across x (radially) along the whole length of the X-line (localized in the region $-40 < y/d_e < 0$), as can be seen at $\omega_{ce}t = 5$ in Fig. 3. On the other hand, J_y sharpens radially and intensifies in the region of localization. This opposite behavior of J_y and B_z is explained in Fig. 4 which schematically shows the radial profiles of J_y and B_z before and after reconnection. In the vicinity of X-point at $x = 0$, the reconnection electric field E_y accelerates the electron flow and therefore J_y increases above its initial peak value. The increase in $J_y \propto \frac{\partial B_z}{\partial x}$ requires the radial profile of B_z to become sharper near $x = 0$. The sharpening of B_z -profile near $x = 0$ is facilitated by the incoming upstream magnetic field lines frozen-in with the electron inflow. This increases the magnetic field in the vicinity of $x = 0$ but depletes it in the upstream region. As a result, the B_z -profile flattens in the upstream region while sharpens in the vicinity of $x = 0$. Since $J_y \propto \partial B_z / \partial x$, the flattening of B_z -profile in the upstream region is associated with a drop in the value of J_y and hence thinning of J_y -profile. Therefore, the overall B_z -profile broadens, while the J_y -profile thins down, as illustrated in Fig. 4. Thinning and intensification of J_y at X-points were observed in 2D EMHD simulations³¹ as well. Although J_y intensifies at an X-point, we shall see in Fig. 5 that the total current along y drops.

Further on, the radial broadening of B_z spreads in the direction of the electron drift velocity (y), qualitatively similar to the spreading observed in MRX.²¹ This extends the X-line as well. The propagation front reaches from $y/d_e \approx 5$ at $\omega_{ce}t = 15$ to $y/d_e \approx 15$ at $\omega_{ce}t = 25$, giving an average speed close to the peak electron flow speed $V_0/v_{Ae} = 1$. Note that the propagation of the reconnection structure is similar to the "reconnection wave" propagation observed in Hall-MHD simulations²³ and in 3D PIC simulations.^{25,26}

The formation and extension of an X-line along with the radial broadening of B_z are associated with current disruption and its spreading. Fig. 5 shows the spreading of the current disruption along y . The magnitude of the total current $I_{y,\text{total}}(y, t) = \int_{-l_x}^{l_x} \int_{-l_z/2}^{l_z/2} J_y(x, y, z, t) dx dz$ drops and the magnitude of electric field (E_y) at the X-line rises with time first in the region $-40 < y/d_e < 0$, where the perturbation is initially localized. At a given location, $y/d_e > 0$, $I_y = |I_{y,\text{total}}|$

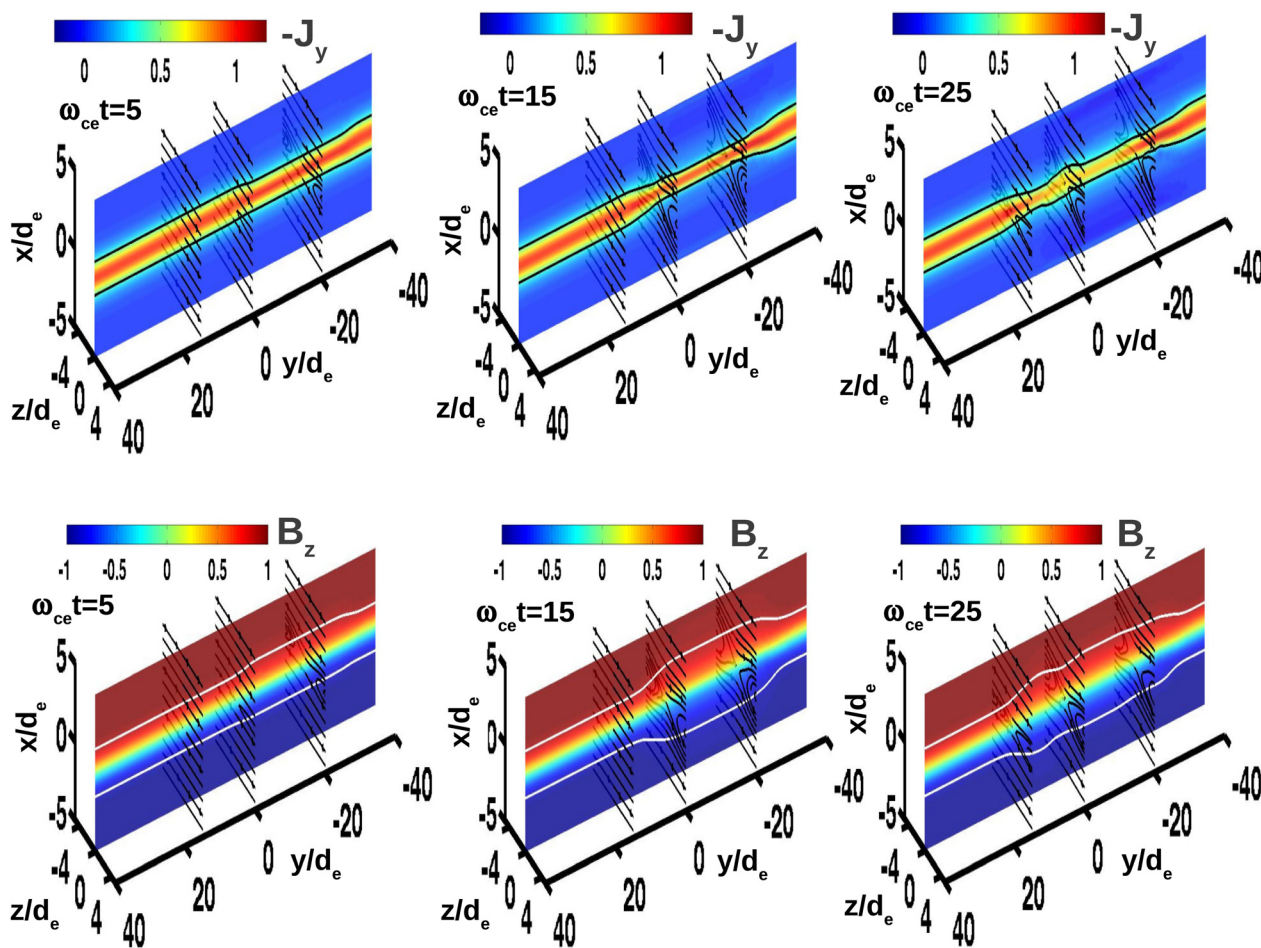


FIG. 3. (3D EMHD simulation result) Evolution of the out-of-reconnection-plane current J_y (top row) and B_z (bottom row) in the $z = 0$ plane with projection of magnetic field lines (black) in the planes $y/d_e = -20, 0,$ and 15 for an initial reconnection perturbation localized in the region $-40 < y/d_e < 0$. Contour lines in the plane $z = 0$ for $J_y/n_0ev_{Ae} = -0.4$ (top row, black lines) and $B_z/B_\infty = -0.9, 0.9$ (bottom row, white lines) show how the thinning of J_y and broadening of B_z in the vicinity of X-line spreads along y .

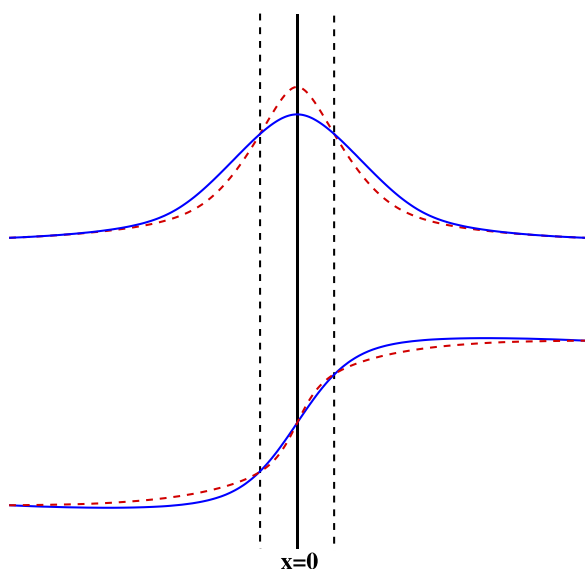


FIG. 4. Schematic representation of the profiles of $-J_y$ (top) and B_z (bottom) before (blue-solid) and after (red-dash) reconnection. The vertical solid line aligns the peak of J_y and zero crossing of B_z . The region of the intensification of J_y is shown between two vertical dashed lines.

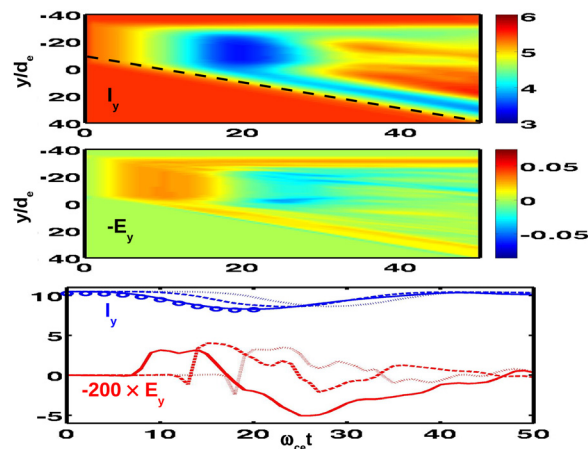


FIG. 5. Spreading of the current disruption along y for the current sheet initialized with a y -localized perturbation. Magnitude of the total current along y ($I_y = |I_{y,total}|$) (top panel) and electric field ($-E_y$) at X-point (middle plane) as a function of y and time. In the bottom panel, $-200 \times E_y$ (red) and I_y (blue) for $y = 0$ (solid), $y = 5d_e$ (dash), and $y = 10d_e$ (dot). Blue circles represent magnitude of the total current $I_{y,total} = I_{y1} + I_{y2}$ calculated using normalized versions of Eqs. (4) and (6) for $y = 0$.

remains constant at its initial value and $E_y \approx 0$ until the X-line is extended to that location allowing I_y to drop and the magnitude of E_y at the X-line to rise (cf. the bottom panel of Fig. 5, showing the evolution of I_y and $-E_y$ at different locations along y). The slope of the dashed line in the top panel of Fig. 5 provides the speed of spreading as $\sim v_{Ae}$. Note that for $y/d_e > -20$ the total current I_y rises again after $\omega_{ce}\Delta t \sim 20$ after the initial drop. Due to the periodic boundary conditions along z (the reconnection-outflow direction), the simulations are reliable only until the outflow recirculates back to the X-line. The typical outflow speed is $\sim 0.5v_{Ae}$. Hence, the simulation box size along z ($\sim 10d_e$) gives time of recirculation of $\sim 20\omega_{ce}^{-1}$. This determines the period of the validity of the simulation results after the arrival of the perturbation at a given y -location.

Although the drop in the current in a $y = \text{constant}$ ($x-z$) plane is delayed by the time, it takes the X-line to reach there, the amount of drop is almost the same. An estimate of the current drop can be obtained from the bottom panel in Fig. 5 as being about $\approx 30\%$. After the electric field ($-E_y$) first attains a small negative value, it rises to a positive peak value which is close to the time when the ankle of the current drop is reached. The negative value becomes larger farther away from $y=0$ plane but the positive peak value is similar at all distances along y .

In the bottom panel of Fig. 5, the magnitude of the total out-of-plane current $I_{y,\text{total}} = I_{y1} + I_{y2}$ is also shown. Here the values of I_{y1} and I_{y2} are calculated from the normalized versions of Eqs. (4) and (6) using values of L' , $B_{x,\text{peak}}$, and δ estimated from the simulation profiles of $B_x(x, 0, l_z/2, t)$. There is a good agreement between the current obtained directly from the simulations and the current calculated using the analytic expressions (blue circles in the bottom panel of Fig. 5).

B. Sinusoidal perturbation with single wavelength along y

One of the observations in MRX²¹ was that the radial profile of B_z gets sharper when a flux rope (winding around the O-points) builds up and broadens, while it is ejected away from an X-point. In simulations initialized with localized perturbations, however, only X-line can form. In order to study the 3D structure of B_z near both X- and O-points, as well as the transition between O- to X-points, we performed another set of simulations which were initialized by a sinusoidal perturbation ($g(y) = \sin(\pi y/l_y)$) with a single wavelength of $2l_y = 20d_e$ along y .

Fig. 6 shows the resulting evolution of the current density ($-J_y$) in the $x-z$ ($y/d_e = -10, 0, 10$) planes. Because of the initial sinusoidal perturbation, in the $y=0$ plane an X-point, while in the planes $y/d_e = -10$ and $y/d_e = 10$ O-points are formed in the center at $\omega_{ce}t = 10$. By $\omega_{ce}t = 30$, the X-point in the plane $y=0$ is replaced by an O-point while the former O-points are replaced by X-points (at $y/d_e = -10$ and $y/d_e = 10$). The magnetic field topology changes back from X- to O-points and O- to X-points at $\omega_{ce}t = 50$. The transformation from X- to O-points and vice versa in different $x-z$ planes is due to the convection of the magnetic field frozen into the electrons flowing along the y -direction. Since the O-point is convected from the mid-plane $y=0$ at $\omega_{ce}t = 30$ to the end plane $y/d_e = 10$ at $\omega_{ce}t = 50$, the speed of its propagation is about $\approx 0.5v_{Ae}$.

Fig. 7 shows iso-surfaces of the total magnetic field for $B/B_\infty = 0.15$ colored by $-J_y$. The high values (red) of $-J_y$ at the X-points follow a kinked line on the iso-surface and show that reconnection takes place through a kinked current sheet. The magnetic field lines illustrate the topology of 3D reconnection near 3D extension of X- and O-points.

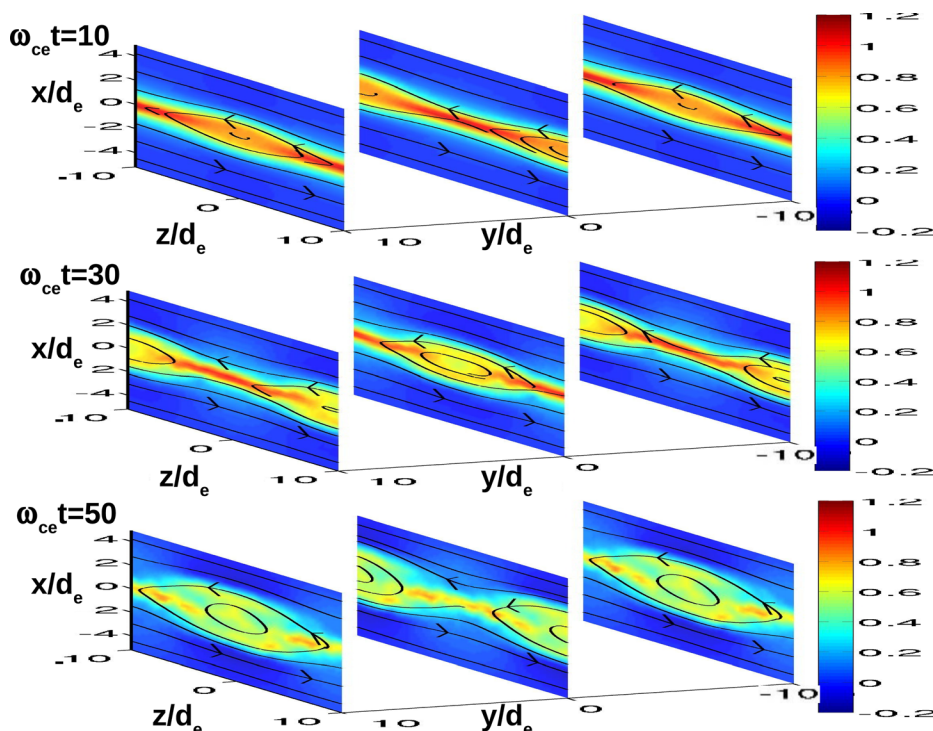


FIG. 6. Dynamical evolution of the current density ($-J_y$) (color) and projection of magnetic field (black lines) in $x-z$ planes. Simulations are initialized by a sinusoidal perturbation with a single wavelength of $2l_y = 20d_e$ along y .

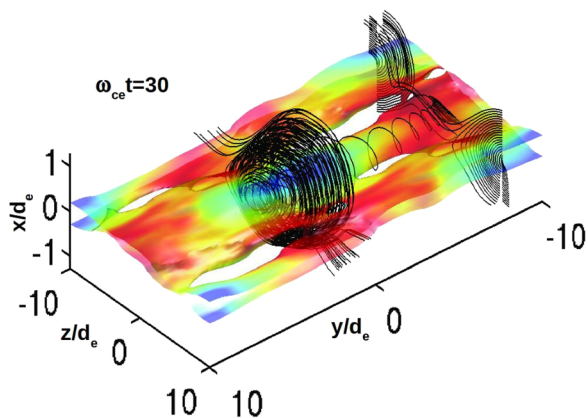


FIG. 7. Iso-surface of the total magnetic field ($B/B_\infty = 0.15$) colored by the current density ($-J_y$) (blue: minimum, red: maximum) at $\omega_{ce}t = 30$. Magnetic field lines (black) illustrate the 3D topology of the magnetic field around O- and X-points.

Figs. 8(a) and 8(b) show color plots of B_z in the plane $z = 0$ at $\omega_{ce}t = 30$ and 50. The X- and O-points are marked in the planes $y/d_e = -10, 0, 10$. The radial profiles of B_z in Fig. 8 are broader at X-points and sharper at O-points, e.g., as evident from the contour lines $B_z/B_\infty = -0.9$ and 0.9 . The radial profiles of B_z along the line $z = 0$ in the central $x-z$ plane ($y = 0$) in Fig. 8(d) show that the overall B_z -profile is broader (sharper) at $\omega_{ce}t = 50$ ($\omega_{ce}t = 30$) when the plane $y = 0$ contains the X-point (O-point). On the other hand, J_y in Fig. 6 exhibits the opposite behavior, viz., a radial broadening (thinning) at the O-point (the X-point). Thinning and intensification of J_y at X-points are schematically illustrated in Fig. 4 and have been explained in Sec. IV A.

The radial broadening of B_z spreads along y as can be seen in Figs. 8(a) and 8(b). It is due to the convection of magnetic field frozen into the electron flow. The radial profile of B_z is broader at $\omega_{ce}t = 30$ in the $y/d_e = -10$ plane

where an X-point is located at that time. At $\omega_{ce}t = 50$, the broadening spreads to the $y = 0$ plane due to the movement of the X-point to there.

Note that the current disruption in MRX is associated with the ejection of a flux rope in the $x-z$ plane. This changes the magnetic field configuration in the $x-z$ plane from O-point to X-point. In our 3D simulations, magnetic field configuration in $x-z$ planes changes from O- to X-point due to the propagation along y . In Figs. 8(a) and 8(b), the O-point in the plane $y = 0$ at $\omega_{ce}t = 30$ is propagated away and at its position an X-point appears at $\omega_{ce}t = 50$. The total current through an area ($-10 < x/d_e < 10, -5 < z/d_e < 5$) in $y = 0$ plane drops during the period $\omega_{ce}t = 30-50$ and magnitude of the electric field E_y at $x = y = z = 0$ rises (as shown between the two dashed vertical lines in Fig. 8(c)), constituting a current disruption event. The simulations cannot be trusted beyond $\omega_{ce}t = 50$ as from that time on the periodic boundaries affect the internal solution (see discussion in Sec. IV A). The drop in the current is small ($< 10\%$) because the X-point in the plane $y = 0$ changes into an O-point after $\omega_{ce}t = 50$. This lets the current to drop only for a short time during which the X-point is active. Note that the drop in the current could be larger if the X-point continued to be active and generate reconnected magnetic field for a longer time.

C. Speed of spreading

In case of localized perturbation, the speed v_{sp} , at which the reconnection region moved in the y -direction, is close to the electron flow speed ($V_0 = v_{Ae}$). In case of sinusoidal perturbation, it is smaller, approximately equal to $0.5 V_0$. It seems that v_{sp} depends on k_y and k_z which are different in the two cases. Past studies in the absence of guide field found the unidirectional speed of X-line spreading to be the drift speed of the current carriers^{23,24} or waves^{25,26} but did not

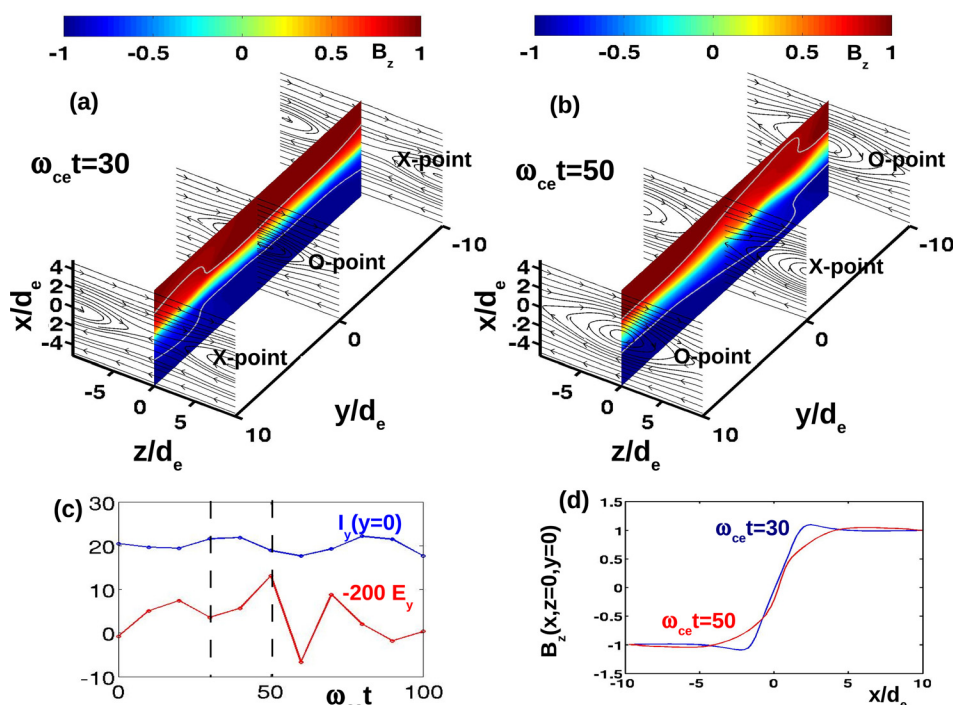


FIG. 8. Color coded B_z and contour lines (white line) for $B_z/B_\infty = -0.9, 0.9$ in the plane $z = 0$ at (a) $\omega_{ce}t = 30$ and (b) $\omega_{ce}t = 50$ with magnetic field lines (black) in the planes $y/d_e = -10, 0, 10$. Electric field ($-200 \times E_y$, red) and total current along y (blue) crossing the area ($-10 < x/d_e < 10, -5 < z/d_e < 5$) in the plane $y = 0$ (c). Radial profiles of B_z along the line $y = z = 0$ (d).

consider the dependence on wave numbers. In the presence of strong guide field, Alfvén waves excited in the guide field spreads the X-line bi-directionally with Alfvén speed.³²

The speed of spreading by the so called “reconnection waves” was obtained in absence of guide field by applying approximate linear EMHD equations near the mid plane $x=0$, ignoring electron inertia.²³ We carry out an eigenvalue analysis of a more general set of linear EMHD equations to understand the wavenumber dependence of v_{sp} . The linear EMHD equations can be written as two coupled equations for the perturbed variables v_{x1} and B_{x1} (Ref. 33)

$$\frac{d^2 v_{x1}}{dx^2} - (1+k^2)v_{x1} + \frac{k_z B_{x1}}{a} + \frac{k_z^2 B_0 v_{x1}}{\bar{\omega} a} + \frac{(v''_0 - v_0)k_y v_{x1}}{\bar{\omega}} = 0, \quad (10)$$

$$a \frac{d^2 B_{x1}}{dx^2} - a(1+k^2)B_{x1} - k_z v_{x1} = 0. \quad (11)$$

Equations (10) and (11) have been Fourier transformed in y , z , and t and written in normalized variables. Here, $a = \bar{\omega} / (B_0 - B''_0)$, $\bar{\omega} = \omega - k_y v_0$, and $k^2 = k_y^2 + k_z^2$. Equations (10) and (11) take into account the full spatial dependence of the equilibrium variables and the electron inertia. Applying Eq. (11) near the mid plane $x=0$, where $v_{x1}=0$, we can obtain the speed of the reconnection wave $\omega/k_y = v_0$ to be the electron drift speed. A full solution of Eqs. (10) and (11), however, contains number of other modes and possibilities for a range of propagation speeds.

Numerically solving Eqs. (10) and (11), one finds a number of unstable modes for given k_y and k_z . In Fig. 9, the k_y and k_z dependence of the y -component of the phase velocity $v_{\phi,y} = \omega_r/k_y$ (where ω_r is real part of the complex eigenvalue $\omega = \omega_r + i\gamma$) is shown for $0 < k_y d_e, k_z d_e \leq 1$ for the

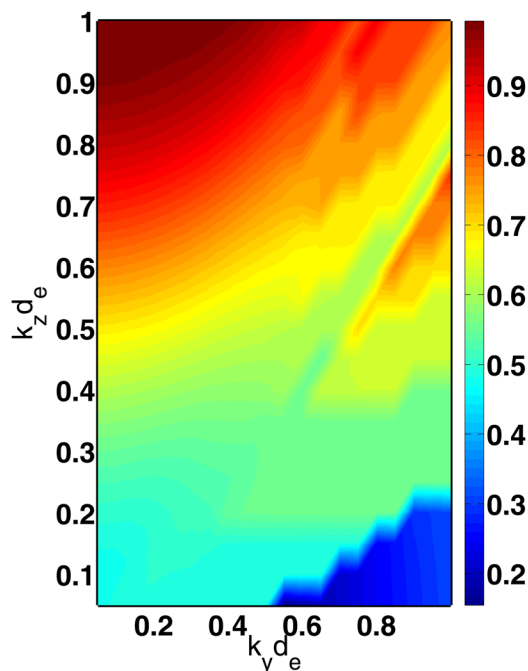


FIG. 9. Color coded y -component of the phase velocity $v_{\phi,y} = \omega_r/k_y$ of the fastest growing mode as a function of k_y and k_z for $L/d_e = 1$.

fastest growing mode. It can be seen that the phase velocity depends on k_y and k_z . Most of the modes with $v_{\phi,y} \approx v_{Ae}$ have $k_z > k_y$. On the other hand, although all modes with $k_z < k_y$ do propagate along y , they have relatively small phase velocities. The dependence of the spreading speed on k_y is consistent with the physical mechanism of spreading proposed by Dorfman *et al.*²¹ Their mechanism also depends on the finite gradients ($\partial v_y/\partial y$) along y . Detailed studies on dependence of spreading speed on k_y , k_z , and L will be presented in future publications.

The simulations initialized with the sinusoidal perturbation have $k_y d_e = k_z d_e = 0.314$. For these values of k_y and k_z , numerical solution of linear EMHD equations gives $\omega_r/k_y \approx -0.6v_{Ae}$, in close agreement with the observed value in the simulations. For the localized perturbation, $k_z d_e = 0.628$. The power is distributed in many k_y and maximizes for the minimum $k_y d_e = \pi/l_y = 0.0785$ in the system. For this set of the values of k_y and k_z , numerical solution gives $\omega_r/k_y \approx -0.89v_{Ae}$, which, again, is in close agreement with the value obtained by the EMHD simulations.

V. CONCLUSION AND DISCUSSION

It has been shown that current disruption is an intrinsic property of the dynamic formation of an X-point in magnetic reconnection, independent of a particular plasma model or of the dimensionality of the system (2D or 3D). This supports recent Hall MHD simulations which show that current disruption in Earth’s magnetotail occurs due to the onset of magnetic reconnection leading to the formation of a magnetic X-point.³⁴ In MRX experiments²¹ also, most of the current disrupts during the formation of an X-point configuration of magnetic field during the ejection of a flux rope. The expression for the current drop, derived from first principles considering a typical X-point magnetic field configuration, agrees well with the current drop obtained by both 2D and 3D EMHD simulations.

Three-dimensional EMHD simulations initialized with a reconnection perturbation localized along y (in half the simulation box) show that an initially localized X-line extends in the direction of the electron flow. This also spreads the radial broadening of B_z and the associated current disruption in the direction of the electron flow. Simulations initialized with a sinusoidal (along y) reconnection perturbation show that the magnetic field geometry in the $x-z$ planes changes along y from X-point to O-point and vice-versa. The wavelength of the variation of the geometry is equal to the wavelength of the perturbation (λ), i.e., X-point changes to O-point and then to X-point again in a single wavelength of the perturbation. The reconnection structure propagates in time along y with a wavenumber dependent speed (v_{sp}). The patterns of alternating X- and O-points are maintained in the course of the propagation of the reconnection structure in the y -direction, being carried along with the electron flow. In a given $x-z$ plane, the time period of change from X-point to O-point to X-point is λ/v_{sp} . The overall profile of B_z across the width of the current sheet is broader at X-point than at an O-point position, although it is sharper at an X-point near the center of the current sheet.

In the MRX reconnection experiment,²¹ both current disruption and its spreading along y were observed: the total current, which crosses the plane $y=0$, drops approximately by 37% (from 8 kA at $t=330\ \mu\text{s}$ to 5 kA at $t=334\ \mu\text{s}$) in about $4\ \mu\text{s}$. Using Eq. (7) and typical MRX parameters ($L' \approx 3.5\ \text{cm}$, $z_2 - z_1 = 18\ \text{cm}$, $B_{x,\text{peak}}(z_2) \approx 112\ \text{G}$, and $B_\infty \approx 300\ \text{G}$), the estimate of the current drop $\Delta I_{y,\text{total}}$ is approximately 29%. The MRX parameters used in Eq. (7) for the estimation of the current drop were obtained by approximately fitting the experimental profile of B_x at $z=9\ \text{cm}$ and $t=334\ \mu\text{s}$ to the profile given by Eq. (5). This estimate of the current drop is similar to the experimentally observed drop in the total current. Simultaneous with the drop in the current, the out-of-plane electric field E_y at the X-point rises from $\sim 2\ \text{V/cm}$ to $\sim 4\ \text{V/cm}$. The reconnection rate $E_y \sim 2\ \text{V/cm}$ before current disruption depends on the time dependent plasma currents and the external coil currents. The plasma currents are due to details of the plasma creation and discharge evolution processes in MRX which are beyond the scope of the present paper. A rough estimate of the magnitude of the electric field due to the main coil current ramp-down can be made using Faraday's law $\oint \mathbf{E} \cdot d\mathbf{l} = -\frac{d\phi}{dt}$, where the line integral is over a circle of radius R centered at the axis of the two current coils and located right in middle of them. The flux of the magnetic field $\phi = \int \mathbf{B} \cdot d\mathbf{s} \approx B_{av} \pi R^2$ is estimated using an average value of the magnetic field B_{av} over the area enclosed by the circle of radius R . The magnetic field due to the two current coils varies along the radius of the circle from B_{axis} at the center to $0.4B_{axis}$ at the coil radius. So, the average magnetic field over the area of the circle can be approximated as $0.7B_{axis}$, where $B_{axis} = \mu_0 I_{coil} R_{coil}^2 / (R_{coil}^2 + z^2)^{3/2}$. Here, R_{coil} is the radius of the two coils each carrying current I_{coil} and separated by a distance $2z$. The component E_y can be written as

$$E_y = -0.35 \times \frac{\mu_0 R R_{coil}^2}{(R_{coil}^2 + z^2)^{3/2}} \frac{dI_{coil}}{dt}.$$

For MRX parameters ($R \sim R_{coil} = 0.375\ \text{m}$, $z = 0.294\ \text{m}$, and $dI_{coil}/dt \approx 500\ \text{MA/s}$), one obtains $E_y = 1.07\ \text{V/cm}$, which is of the same order of magnitude as the peak vacuum $E_y \sim 1.5\ \text{V/cm}$ in MRX³⁵ for typical discharge parameters.

The rise in the magnitude of E_y during current disruption is due to the onset of faster magnetic reconnection at $t=330\ \mu\text{s}$, which allows a faster removal of B_z from the circular area of radius R . The rate of the removal of B_z is equal to the rate of the generation of B_x and can be estimated as follows. Neglecting gradients along y , the x -component of Faraday's law gives $\partial E_y / \partial z \approx \partial B_x / \partial t$. Integrating along the line $x \approx 38\ \text{cm}$ from $z=0$ to $z=9\ \text{cm}$, we get $E_y|_{z=0} = E_y|_{z=9\ \text{cm}} - \Delta z [\partial / \partial t (\int B_x(x, z) dz / \Delta z)]$, where $\Delta z = 9\ \text{cm}$. In MRX, the value of B_x averaged over the distance $\Delta z = 9\ \text{cm}$ ($0 < z < 9\ \text{cm}$) increases from ~ 0 at $t=330\ \mu\text{s}$ to $\sim 75\ \text{G}$ at $t=334\ \mu\text{s}$ (see Fig. 2(d) in Dorfman *et al.*²¹). This gives $[\partial / \partial t (\int B_x(x, z) dz / \Delta z)]_{t=332\ \mu\text{s}} \sim 75\ \text{G} / 4\ \mu\text{s} = 1875\ \text{T/s}$. Substituting for $E_y|_{z=9\ \text{cm}}$ the experimental value $\approx -2\ \text{V/cm}$ at $t=332\ \mu\text{s}$ (see Fig. 2(b) in Dorfman *et al.*²¹), we get $E_y|_{z=0} \approx -3.69\ \text{V/cm}$. At $t=330\ \mu\text{s}$, the experimental value of

$E_y|_{z=0} \approx -2\ \text{V/cm}$, therefore, the rise in the magnitude of E_y at the X-point ($z=0$) is $1.69\ \text{V/cm}$ by $t=332\ \mu\text{s}$. This is consistent with the experimental results.

The spreading of the current disruption along y , observed in the simulations, is qualitatively similar to the one observed in MRX. The speed of spreading in MRX is about $\approx 5\ \text{cm}/\mu\text{s}$.³⁵ This is a fraction of the electron drift speed estimated as $J_y / ne \approx 30\ \text{cm}/\mu\text{s}$ ($n = 2 \times 10^{13}\ \text{cm}^{-3}$ and assuming that the current is carried mainly by electrons). A linear eigen-value analysis of EMHD equations showed that the speed of spreading can be a fraction of the electron drift speed depending upon the wave numbers k_y and k_z .

Although we do observe a commonality of features indicating the same principal physical effects in EMHD simulations and MRX experiments, the simulations presented here do not directly correspond to the experimental setup. In experiments, the current layer before disruption is thicker (half thickness $\sim 1\ \text{cm} \approx 6d_e$). The Sweet-Parker thickness $\delta_{SP} = L_z / \sqrt{S} \sim 3 - 20\ \text{mm} \geq d_e$ implies a finite resistivity in the electron scale current sheet. Reconnection is driven and there are finite gradients in density and magnetic field along the current direction. Simulations that include some of these features are needed to provide more detailed descriptions of the experimental results. On the other hand, new experiments in MRX can be setup based on the EMHD simulations results. For example, modes with a spectrum of wavelengths along y can be excited in EMHD regime and the wave number dependence of the speed of propagation can be directly verified. This would, however, require the implementation of an array of probes to scan the 3D magnetic field instantaneously and to distinguish between temporal and spatial variations.

We emphasize that the present manuscript focuses on the current disruption and its spreading along y . It does not address the mechanisms of impulsive reconnection which includes both the slow build up and disruption phases. Models describing impulsiveness and effect of resistivity has been developed by other authors,^{8,34,36-38} for example, a model of the transition from slow to fast reconnection below a critical resistivity.³⁶ The message here in this paper is that current disrupts with the formation of a magnetic X-point in reconnection independent of what triggers the reconnection to form an X-point. Of course, the extent and time scale of current disruption may depend on the trigger mechanisms and physical processes occurring in the system.

In conclusion, the similarity of the basic features of MRX reconnection and EMHD simulations indicates that the essential physics of current disruption is captured by describing the electron flow dynamics. This motivates more complicated 3D EMHD simulations closer to the experimental conditions. The results of such simulations will be presented in future publications.

ACKNOWLEDGMENTS

The work of N.J. was funded by the Max-Planck/Princeton Center for Plasma Physics (Grant No. M.MC.A.Aero8003 Max Planck) and the NSF grant (AGS 1027185) to the University of Maryland. The work of A. S. Sharma was funded by the NSF

grant (AGS 1027185) to the University of Maryland. S.D. was supported by a DOS FES Fellowship and the NDSEG Fellowship Program (Contract No. DE-AC02-09CH11466). The MPS authors (N.J. and J.B.) thank Dr. Bernhardt Bandow for his help to numerically optimize the EMHD code.

- ¹P. A. Sweet, in *Electromagnetic Phenomena in Cosmical Physics*, edited by B. Lehnert (Cambridge University Press, New York, 1958), p. 123.
- ²E. N. Parker, "Sweet's mechanism for merging magnetic fields in conducting fluids," *J. Geophys. Res.* **62**, 509, doi:10.1029/JZ062i004p00509 (1957).
- ³D. Biskamp, "Magnetic reconnection via current sheets," *Phys. Fluids* **29**, 1520 (1986).
- ⁴H. E. Petschek, in *AAS/NASA Symposium on the Physics of Solar Flares*, edited by W. N. Hess (NASA, Washington, DC, 1964), p. 425.
- ⁵S. I. Syrovatsky, "Formation of current sheets in a plasma with a frozen-in strong magnetic field," *Sov. Phys. JETP* **33**, 933 (1971).
- ⁶J. Birn, J. F. Drake, M. A. Shay, B. N. Rogers, R. E. Denton, M. Hesse, M. Kuznetsova, Z. W. Ma, A. Bhattacharjee, A. Otto, and P. L. Pritchett, "Geospace environmental modeling (GEM) magnetic reconnection challenge," *J. Geophys. Res.* **106**, 3715, doi:10.1029/1999JA900449 (2001).
- ⁷W. Daughton, J. Scudder, and H. Karimabadi, "Fully kinetic simulations of undriven magnetic reconnection with open boundary conditions," *Phys. Plasmas* **13**, 072101 (2006).
- ⁸A. Bhattacharjee, K. Germaschewski, and C. S. Ng, "Current singularities: Drivers of impulsive reconnection," *Phys. Plasmas* **12**, 042305 (2005).
- ⁹W. Daughton, V. Roytershteyn, H. Karimabadi, L. Yin, B. J. Albright, B. Bergen, and K. J. Bowers, "Role of electron physics in the development of turbulent magnetic reconnection in collisionless plasmas," *Nat. Phys.* **7**, 539 (2011).
- ¹⁰B. U. Ö. Sonnerup, *Solar System Plasma Physics* (North-Holland, Amsterdam, 1979), Vol. 3, pp. 47–108.
- ¹¹T. Terasawa, "Hall current effect on tearing mode instability," *Geophys. Res. Lett.* **10**, 475, doi:10.1029/GL010i006p00475 (1983).
- ¹²Y. Ren, M. Yamada, S. Gerhardt, H. Ji, R. Kulsrud, and A. Kuritsyn, "Experimental verification of the Hall effect during magnetic reconnection in a laboratory plasma," *Phys. Rev. Lett.* **95**, 055003 (2005).
- ¹³M. R. Brown, C. D. Cothran, and J. Fung, "Two fluid effects on three-dimensional reconnection in the swarthmore spheromak experiment with comparisons to space data," *Phys. Plasmas* **13**, 056503 (2006).
- ¹⁴F. S. Mozer, S. D. Bale, T. D. Phan, and J. A. Osborne, "Observations of electron diffusion regions at the subsolar magnetopause," *Phys. Rev. Lett.* **91**, 245002 (2003).
- ¹⁵X. H. Deng and H. Matsumoto, "Rapid magnetic reconnection in the earth's magnetosphere mediated by whistler waves," *Nature* **410**, 557 (2001).
- ¹⁶C. T. Russell and R. L. McPherron, "The magnetotail and substorms," *Space Sci. Rev.* **15**, 205 (1973).
- ¹⁷A. T. Y. Lui, in *Magnetospheric Substorms*, Geophysics Monograph No. 64, edited by J. R. Kan, T. A. Potemra, S. Kokubun, and T. T. Lijima (American Geophysical Union, 1991), pp. 43–60.
- ¹⁸A. T. Y. Lui, "Electric current approach to magnetospheric physics and the distinction between current disruption and magnetic reconnection," in *Magnetospheric Current Systems*, edited by S.-I. Ohtani, R. Fujii, M. Hesse, and R. L. Lysak (American Geophysical Union, Washington, DC, 2000).
- ¹⁹N. Katz, J. Egedal, W. Fox, A. Le, J. Bonde, and A. Vrublevskis, "Laboratory observation of localized onset of magnetic reconnection," *Phys. Rev. Lett.* **104**, 255004 (2010).
- ²⁰M. Yamada, "Mechanisms of impulsive magnetic reconnection: Global and local aspects," *Phys. Plasmas* **18**, 111212 (2011).
- ²¹S. Dorfman, H. Ji, M. Yamada, J. Yoo, E. Lawrence, C. Myers, and T. D. Tharp, "Three-dimensional, impulsive magnetic reconnection in a laboratory plasma," *Geophys. Res. Lett.* **40**, 233, doi:10.1029/2012GL054574 (2013).
- ²²Y. Ono, M. Inomoto, T. Okazaki, and Y. Ueda, "Experimental investigation of three-component magnetic reconnection by use of merging spheromaks and tokamaks," *Phys. Plasmas* **4**, 1953 (1997).
- ²³J. D. Huba and L. I. Rudakov, "Three dimensional hall magnetic reconnection," *Phys. Plasmas* **9**, 4435 (2002).
- ²⁴G. Lapenta, D. Krauss-Varban, H. Karimabadi, J. D. Huba, L. I. Rudakov, and Paolo Ricci, "Kinetic simulations of x-line expansion in 3-d reconnection," *Geophys. Res. Lett.* **33**, L10102, doi:10.1029/2005GL025124 (2006).
- ²⁵J. Büchner and J. P. Kuska, "Numerical simulation of three dimensional reconnection due to the instability of collisionless current sheets," *Adv. Space Res.* **19**, 1817 (1997).
- ²⁶J. Büchner and J. P. Kuska, "Sausage mode instability of thin current sheets as a cause of magnetospheric substorms," *Ann. Geophys.* **17**, 604 (1999).
- ²⁷S. V. Bulanov, F. Pegoraro, and A. S. Sakharov, "Magnetic reconnection in electron magnetohydrodynamics," *Phys. Fluids B* **4**, 2499 (1992).
- ²⁸M. Hesse and D. Winske, "Electron dissipation in collisionless magnetic reconnection," *J. Geophys. Res.* **103**, 26479, doi:10.1029/98JA01570 (1998).
- ²⁹L. R. Lyons and D. C. Pridmore-Brown, "Force balance near an x-line in a collisionless plasma," *J. Geophys. Res.* **95**, 20903, doi:10.1029/JA095iA12p20903 (1990).
- ³⁰M. Kuznetsova, M. Hesse, and D. Winske, "Collisionless reconnection supported by nongyrotropic pressure effects in hybrid and particle simulations," *J. Geophys. Res.* **106**, 3799, doi:10.1029/1999JA001003 (2001).
- ³¹N. Jain, A. Surjalal Sharma, L. M. Zelenyi, and H. V. Malova, "Electron scale structures of thin current sheets in magnetic reconnection," *Ann. Geophys.* **30**, 661 (2012).
- ³²L. S. Shepherd and P. A. Cassak, "Guide field dependence of 3-D X-line spreading during collisionless magnetic reconnection," *J. Geophys. Res.* **117**, A10101, doi:10.1029/2012JA017867 (2012).
- ³³N. Jain, A. Das, and P. Kaw, "Kink instability in electron magnetohydrodynamics," *Phys. Plasmas* **11**, 4390 (2004).
- ³⁴Z. W. Ma, "Sudden disruption of the cross-tail current in the magnetotail," *Phys. Plasmas* **15**, 032906 (2008).
- ³⁵S. Dorfman, "Experimental study of 3-D, impulsive reconnection events in a laboratory plasma," Ph.D. thesis (Princeton University, Princeton, 2012).
- ³⁶P. A. Cassak, M. A. Shay, and J. F. Drake, "Catastrophe model for fast magnetic reconnection onset," *Phys. Rev. Lett.* **95**, 235002 (2005).
- ³⁷P. A. Cassak, J. F. Drake, and M. A. Shay, "A model for spontaneous onset of fast magnetic reconnection," *Astrophys. J.* **644**, L145 (2006).
- ³⁸A. Bhattacharjee, Z. W. Ma, and X. Wang, "Impulsive reconnection dynamics in collisionless laboratory and space plasmas," *J. Geophys. Res.* **104**, 14543, doi:10.1029/1998JA900094 (1999).